0026-895X/11/7904-710–723$20.00
MOLECULAR PHARMACOLOGY
Vol. 79, No. 4
70045/3677947
Mol Pharmacol 79:710–723, 2011
Printed in U.S.A.

A Novel Defensive Mechanism against Acetaminophen Toxicity in the Mouse Lateral Nasal Gland: Role of CYP2A5-Mediated Regulation of Testosterone Homeostasis and Salivary Androgen-Binding Protein Expression

Xin Zhou, Yuan Wei, Fang Xie, Christina M. Laukaitis, Robert C. Karn, Kerri Kluetzman, Jun Gu, Qing-Yu Zhang, Dean W. Roberts, and Xinxin Ding

Wadsworth Center, New York State Department of Health, and School of Public Health, State University of New York at Albany, Albany, New York (X.Z, Y.W., F.X., K.K., J.G., Q.-Y.Z., X.D.); College of Medicine, University of Arizona, Tucson, Arizona (C.M.L., R.C.K.); and Department of Pediatrics, University of Arkansas for Medical Sciences, Little Rock, Arkansas (D.W.R.)

Received November 16, 2010; accepted January 19, 2011

ABSTRACT

To identify novel factors or mechanisms that are important for the resistance of tissues to chemical toxicity, we have determined the mechanisms underlying the previously observed increases in resistance to acetaminophen (APAP) toxicity in the lateral nasal gland (LNG) of the male *Cyp2g1*-null/*Cyp2a5*-low mouse. Initial studies established that *Cyp2a5*-null mice, but not a newly generated strain of *Cyp2g1*-null mice, were resistant to APAP toxicity in the LNG; therefore, subsequent studies were focused on the *Cyp2a5*-null mice. Compared with the wild-type (WT) male mouse, the *Cyp2a5*-null male mouse had intact capability to metabolize APAP to reactive intermediates in the LNG, as well as unaltered circulating levels of APAP, APAP-GSH, APAP-glucuronide, and APAP-sulfate. However, it displayed reduced tissue levels of APAP and APAP-GSH and increased tissue levels of testosterone and salivary androgen-binding protein (ABP) in the LNG. Furthermore, we found that ABP was able to compete with GSH and cellular proteins for adduction with reactive metabolites of APAP in vitro. The amounts of APAP-ABP adducts formed in vivo were greater, whereas the amounts of APAP adducts formed with other cellular proteins were substantially lower, in the LNG of APAP-treated male *Cyp2a5*-null mice compared with the LNG of APAP-treated male WT mice. We propose that through its critical role in testosterone metabolism, CYP2A5 regulates 1) the bioavailability of APAP and APAP-GSH (presumably through modulation of the rates of xenobiotic excretion from the LNG) and 2) the expression of ABP, which can quench reactive APAP metabolites and thereby spare critical cellular proteins from inactivation.

Introduction

Acetaminophen (APAP) is widely used as a model compound for studying the mechanisms of chemical toxicity. In mice, APAP causes toxicity in several organs, including the liver, kidney, lung, the nasal olfactory mucosa and respiratory mucosa, and the lateral nasal gland (LNG) (Zhuo et al., 2004; Gu et al., 2005). The LNG, found in most mammalian species, including humans, is one of the largest anterior nasal glands (Moe and Bojsen-Moller, 1971). The gland is believed to play important roles in the sense of smell through secretion of odorant binding proteins (Pes et al., 1998) and in the immune barrier function of the olfactory mucosa through secretion of immunoglobulin A (Getchell and Mellert, 1991).

The metabolic basis of APAP toxicity in the liver is reasonably well understood (for review, see Hinson et al., 2004). P450-mediated metabolic activation of APAP generates a toxic intermediate, *N*-acetyl-*p*-benzoquinoneimine, that can be detoxified via conjugation with cellular GSH. Under overdose conditions, there is greater formation of *N*-acetyl-*p*-

This work was supported in part by the National Institutes of Health National Institute of Environmental Health Sciences [Grant ES007462] (to X.D.); the National Institutes of Health National Institute of Diabetes and Digestive and Kidney Diseases [Grant DK081406] (to D.W.R.); the Arkansas Children's Hospital Research Institute and the Arkansas Biosciences Institute, the major research component of the Tobacco Settlement Proceeds Act of 2000 (to D.W.R.); the National Institutes of Health National Cancer Institute/University of Arizona SPORE in GI Cancer [Grants CA95060, CA023074] (to C.M.L.); and the National Institutes of Health National Institute of Child Health and Human Development [Grant 5F33-HD055016-02] (to R.C.K.).

Article, publication date, and citation information can be found at http://molpharm.aspetjournals.org.

doi:10.1124/mol.110.070045.

ABBREVIATIONS: APAP, acetaminophen; P450, cytochrome P450; PCR, polymerase chain reaction; HPLC, high-performance liquid chromatography; LC-MS, liquid chromatography-mass spectrometry; LNG, lateral nasal gland; APAP-G, acetaminophen-glucuronide; APAP-S, acetaminophen-sulfate; ABP, salivary androgen-binding protein; WT, wild type; B6, C57BL/6; kbp, kilobase pair(s); ES, embryonic stem; E2-Glu, 17β-estradiol-3-(β-D-glucuronide); GAPDH, glyceraldehyde 3-phosphate dehydrogenase.

benzoquinoneimine, which leads to GSH depletion, adduction and inactivation of cellular macromolecules, increased cellular oxidative stress, and eventually cell death.

The mechanisms of APAP toxicity in extrahepatic tissues are complicated by possible contributions from toxic APAP metabolites generated in multiple tissue sources, including the liver and the extrahepatic target organ, such as the lung and the olfactory mucosa, where APAP-metabolizing enzymes are also expressed. The contributions of liver P450 enzymes to APAP toxicity in the kidney, lung, nasal mucosa, and LNG were determined previously through the use of the liver-specific P450 reductase knockout mouse model (Gu et al., 2005). The results of that study indicated that, although APAP toxicity in the olfactory mucosa was independent of APAP metabolic activation in the liver, APAP toxicity in the lung, kidney, and LNG was at least partly dependent on metabolism of APAP by hepatic P450 enzymes.

In mice, CYP2G1 and CYP2A5 are two of the most abundant P450s expressed in the olfactory mucosa (Gu et al., 1998). CYP2A5, but not CYP2G1, is also expressed in the LNG (Zhuo et al., 2004). Heterologously expressed mouse CYP2G1 and CYP2A5 exhibited high activity toward endogenous sex steroid hormones, such as testosterone and progesterone (Gu et al., 1999), and several xenobiotic compounds, including APAP (Gu et al., 1998). In a previously generated *Cyp2g1*-null mouse model (Zhuo et al., 2004), the expression of *Cyp2a5* was suppressed in several tissues, including the liver, kidney, and the LNG, although not in the olfactory mucosa, as a result of the insertion of a neomycin resistance gene in the *Cyp2g1* locus (Zhou et al., 2010); hereafter, we will refer to that mouse strain as *Cyp2g1*-null/*Cyp2a5*-low to avoid confusion with the newly generated *Cyp2g1*-null mouse (in this study) and the *Cyp2a5*-null mouse (Zhou et al., 2010). Unexpectedly, in the male *Cyp2g1*-null/*Cyp2a5*-low mouse, the LNG, but not the olfactory mucosa, was resistant to APAP toxicity; furthermore, the increases in resistance to APAP toxicity did not arise from reduced metabolic activation of APAP in the target tissue (Zhuo et al., 2004). These findings led us to propose that olfactory mucosa CYP2G1 (through a paracrine pathway) or LNG CYP2A5 may indirectly influence resistance of the LNG to chemical toxicity, possibly by regulating gene expression in the LNG through steroid hormones or other endogenous P450 substrates and their metabolites.

The aim of the present study was to test the preceding hypothesis, with a broader goal of identifying novel factors and mechanisms that are important for the resistance of tissues to chemical toxicity. Our initial studies established that male *Cyp2a5*-null mice, but not male *Cyp2g1*-null mice, were resistant to APAP toxicity in the LNG. Meanwhile, a genomic analysis of gene expression changes in the LNG of the male *Cyp2g1*-null/*Cyp2a5*-low mice identified salivary androgen binding protein (ABP) as one of the most highly up-regulated genes. Mouse ABP, a member of the secretoglobin family, is capable of binding sex steroids having the saturated A ring of testosterone with high affinity (Karn 1998). Therefore, subsequent studies were focused on assessing the impact of *Cyp2a5* knockout on APAP metabolism and testosterone homeostasis, and on establishing mechanistic links among CYP2A5, testosterone, ABP, and resistance of LNG to APAP toxicity in the male *Cyp2a5*-null mouse. These studies led to several novel findings related to tissue-specific mechanisms against xenobiotic toxicity in the LNG and, possibly, other secretory glands. The implications of these findings are discussed, followed by the proposal of a novel defensive mechanism against xenobiotic toxicity.

Materials and Methods

Reagents and Animals. Acetaminophen, *p*-acetamidophenyl β-D-glucuronide sodium salt, acetaminophen sulfate potassium salt, β-estradiol 3-(β-D-glucuronide) sodium salt, and NADPH were purchased from Sigma-Aldrich (St. Louis, MO). The sources of testosterone, 16α-hydroxyprogesterone, and all testosterone metabolite standards were the same as described previously (Ding and Coon, 1994; Zhou et al., 2009). 1,2-D_2-testosterone was obtained from Cambridge Isotope Laboratories (Andover, MA). All solvents (acetonitrile, methanol, and water) were of high-performance liquid chromatography (HPLC) grade (Thermo Fisher Scientific, Waltham, MA). All procedures involving animals were approved by the Institutional Animal Care and Use Committee of the Wadsworth Center. Wild-type (WT) C57BL/6J (B6), WT 129/Sv, transgenic *Cyp2g1*-null/*Cyp2a5*-low (on mixed B6 and 129/Sv genetic background (B6N2); Zhuo et al., 2004), *Cyp2g1*-null (on B6 genetic background; see *Generation of the Cyp2g1-Null Mouse*), and *Cyp2a5*-null (on B6 genetic background; Zhou et al., 2010) mice were obtained from breeding stocks maintained at the Wadsworth Center.

Generation of the *Cyp2g1*-Null Mouse. The targeting vector (Fig. 1) was prepared in the pMC-lox-neo-lox vector (Millipore, Billerica, MA), in which the neo was flanked by two loxP sites in the same orientation (i.e., floxed); the same vector was used for the generation of the *Cyp2a5*-null mice (Zhou et al., 2010). A 6.4-kilobase pair (kbp) PstI fragment, encompassing regions upstream of exon 3, and a 8.4-kbp BamHI fragment, consisting of exons 4 to 8 of the *Cyp2g1* gene, were obtained from the mouse bacterial artificial chromosome clone RP24-238K2 (from the B6 strain; BACPAC Resources, Oakland, CA). The two *Cyp2g1* fragments were cloned into the pMC-lox-neo-lox vector, at the ApaI-EcoRV (for the PstI fragment) and NotI-PmeI (for the BamHI fragment) sites after subcloning into a pCR-Script Amp SK(+) vector (Stratagene, La Jolla, CA); the final targeting construct was linearized with ApaI before electroporation into embryonic stem (ES) cells. The Bruce4 (B6-derived) ES cells (Köntgen et al., 1993), kindly provided by Dr. Colin Stewart (National Cancer Institute, Frederick, MD), were used for electroporation at the Transgenic and Knockout Core Facility of the Wadsworth Center. Procedures for ES cell selection and blastocyst injection were essentially the same as described for the generation of the *Cyp2a5*-null mouse (Zhou et al., 2010). Positive ES cell clones were identified using PCR [with primers 5′-actaacgaaagggcaagtttgg-3′ (upstream of the 6.7-kbp PstI fragment) and 5′-cgatctagaggtaccataacttcgt-3′ (within the vector region) and an annealing temperature of 62°C] and confirmed by Southern blot analysis (data not shown) with both internal (a 350-base-pair ApaI-EcoRV fragment within the vector region) and external probes (a 1.2-kbp XbaI fragment upstream of exon 1 of the *Cyp2g1* gene).

ES cells from a homologous recombinant clone (no. 72) were used for subsequent injection into the blastocyst cavity of albino B6(Cg)-Tyrc-2J/J embryos, from which a chimeric male was generated. Adult *Cyp2g1*-null-neo male chimeras were bred with EIIa-Cre (Lakso et al., 1996) female mice (The Jackson Laboratory, Bar Harbor, ME) for Cre recombinase-mediated deletion of the floxed neo gene in zygote. F1 pups that were heterozygous for the *Cyp2g1*-null allele (without neo), which also contained the EIIa-Cre transgene [*Cyp2g1*(+/−)/EIIa-Cre(+/−)], were then bred with B6 female mice to generate *Cyp2g1*(+/−)/EIIa-Cre(−/−) mice. Homozygous *Cyp2g1*-null mice were produced by cross-breeding between heterozygous littermates. CYP2G1 expression was determined by RNA-PCR, with gene-specific PCR primers (5′-ctgaccgtccttcgaaactttggg-3′ and 5′-gggcttgctcatctccacaaagc-3′; annealing temperature of 65°C), which

amplify sequences (~250 base pairs) corresponding to *Cyp2g1* exons 3 and 4; PCR products were validated by sequence analysis.

Microarray Hybridization and Data Analysis. Microarray analysis was performed with use of the Mouse Expression Set 430A GeneChip (Affymetrix, Santa Clara, CA) arrays. Procedures for RNA preparation, array hybridization, and data analysis were essentially identical to those described previously for hepatic gene expression (Weng et al., 2005). Data sets were normalized using GeneChip-robust multichip analysis, and analysis for statistical significance was performed using the unpaired *t* test in the Genetraffic UNO 3.2 software (Iobion Informatics; La Jolla, CA). The averaged change values from multiple chips, for annotated genes with significantly changed expression ($p < 0.05$; change >1.5-fold; compared with both B6 WT and 129/Sv WT strains) were tabulated together with gene symbol and gene name. The array data are accessible through NCBI's GEO Series accession number GSE26056 (http://www.ncbi.nlm.nih.gov/geo/query/acc.cgi?acc=GSE26056).

RNA-PCR Analysis. Tissues were collected between 9:00 and 10:00 AM local time. Total RNA was isolated with the use of the RNeasy Mini kit (QIAGEN, Valencia, CA). All RNA samples were treated with DNase I (Invitrogen, Carlsbad, CA) before reverse transcription. Real-time RNA-PCR was performed according to the general protocol described elsewhere for analysis of P450 gene expression (Zhang et al., 2005), with use of an ABI 7500 Fast Real-Time PCR System and SYBR Green core reagents (Applied Biosystems, Foster City, CA). The PCR primers used were described previously by Wada et al. (2000) for lipocalin-type prostaglandin D_2 synthase or by Zhou et al. (2009) for *Abpa27* and glyceraldehyde 3-phosphate dehydrogenase (GAPDH). PCR products were validated by sequence analysis, and PCR specificity was confirmed by analysis of reaction products on agarose gels. One of the samples was serially diluted for construction of a standard curve. Experiments were performed in duplicate, and the results were corrected on the basis of the levels of GAPDH mRNA present in the same RNA preparation.

In Vivo Studies in Mice. Two- to 3-month-old male mice were given a single intraperitoneal injection of APAP in warm saline (Gu et al., 2005) at ~10:00 AM, after overnight fasting, at a dose of 400 mg/kg. For determination of the levels of APAP, APAP-GSH, acetaminophen-glucuronide (APAP-G), and acetaminophen-sulfate (APAP-S), blood samples were collected by cardiac puncture, and the LNG was dissected as described previously (Zhuo et al., 2004), at 15 min, 1 h, or 2 h after APAP injection. For determination of nonprotein thiols and APAP-protein adducts, mice were killed at 2 h after APAP injection. For histopathological study of APAP toxicity, mice were killed at 24 h after APAP administration, and the nasal tissues were dissected, fixed in Bouin's fixative, and sectioned, essentially as described previously (Zhuo et al., 2004).

Plasma (~10 μl) and LNG from individual mice were used for determination of APAP level according to the method described previously (Gu et al., 2005). Liver from individual mice and pooled LNG from two mice were used for determination of nonprotein thiols, according to the method of Tonge et al. (1998); GSH was used as a standard.

Determination of Plasma and Tissue Levels of APAP-GSH, APAP-G, and APAP-S. LNG from individual mice was homogenized in 1 ml of water. The internal standard, 17β-estradiol-3-(β-D-glucuronide) (E2-Glu), was added to tissue homogenate or diluted plasma samples at 1 ng/ml. The resultant mixture was extracted with an Isolute Extraction Cartridge (C18, 1 ml/100 mg; Biotage, Charlottesville, VA). Samples were eluted from the cartridge with 0.5 ml of methanol, dried with nitrogen, and reconstituted in 20% (v/v) acetonitrile in water for liquid chromatography-mass spectrometry (LC-MS) analysis. Quantification was carried out with use of calibration curves, constructed by adding APAP-GSH, APAP-G, APAP-S, and E2-Glu to untreated mouse plasma or LNG homogenate. E2-Glu was not detected in nonspiked plasma or tissue samples, and recoveries for all four analytes were >70% in the concentration ranges found in the plasma and tissue samples.

An LC-MS system consisting of an Agilent 1200 Series HPLC and an ABI 4000 Q-Trap mass spectrometer (Applied Biosystems) with a 3.5-μm Symmetry C18 column (2.1 × 150 mm; Waters, Milford, MA) was used. The detection method for APAP-G and APAP-S was modified from that described by Lee et al. (2009). The mobile phase consisted of solvent A (0.05% acetic acid in water) and solvent B (acetonitrile). The column was equilibrated with 70% A/30% B; the samples were eluted at a flow rate of 0.25 ml/min with 30% B for 1 min, followed by linear increases from 30% B to 100% B between 2 and 8 min and then by 100% B for 4 min. The retention time was 4.2 min for APAP-G, 12.1 min for APAP-S, and 8.8 min for the internal standard, E2-Glu. The mass spectrometer was operated in the negative ion mode, using electrospray ionization. The parent/product ion pairs of m/z 326/150 (for APAP-G), 230/150 (for APAP-S), and 417/271 (for E2-Glu) were measured in the multiple reaction monitoring scan mode. The parameters for the chamber were as follows: curtain gas, P_g = 30 psi; heated nebulizer temperature, 350°C; ion spray voltage, −4000 V; nebulizer gas, P_g = 50 psi; turbo gas, P_g = 50 psi; declustering potential, −50 V; and entrance potential, −5 V.

APAP-GSH was determined using the same mobile phase, column, and solvent gradient as for the determination of APAP-G and APAP-S. The retention time of APAP-GSH was 9.8 min. The mass spectrometer was operated in the positive mode, using electrospay ionization. The parent/product ion of m/z 457/328 was measured in the multiple reaction monitoring scan mode. The parameters for the chamber were as follows: curtain gas, P_g = 25 psi; heated nebulizer temperature, 400°C; ion spray voltage, 5000 V; nebulizer gas and turbo gas, P_g = 50 psi; declustering potential, 50 V; and entrance potential, 10 V.

Immunoblot Analysis. LNGs from 10 2- to 3-month-old male mice were pooled for preparation of subcellular fractionations. Tissue homogenate, postmitochondrial S9 fraction, cytosol (supernatant fraction after 100,000*g* centrifugation, possibly also containing secretory vesicles and secreted mucus), and microsomal fractions were obtained, essentially as described previously (Ding and Coon, 1990). Immunoblot analysis was performed with the following antibodies: goat anti-rat CYP3A2, rabbit anti-rat P450-reductase, and goat anti-rat 1A1/2 (BD Gentest, Woburn, MA), rabbit anti-human CYP2E1 (Oxford Biomedical Research, Oxford, MI), rabbit anti-mouse CYP2A5 (Gu et al.,1998), rabbit anti-mouse ABP (Dlouhy et al., 1986), and rabbit anti-human lipocalin-type prostaglandin D_2 synthase (Santa Cruz Biotechnology, Santa Cruz, CA). Immunoblot analysis was carried out under reducing conditions (Laemmli 1970) essentially as described previously (Ding and Coon, 1990). The intensity of the detected bands was quantified with the use of a densitometer (Zhuo et al., 2004).

The levels of APAP-protein adducts were determined with a rabbit anti-APAP antibody (Roberts et al., 1987; Potter et al., 1989); the antiserum (diluted 1/1000 with phosphate-buffered saline plus 0.5% Tween 20) was preincubated with 20 μg of S9 protein from saline-treated B6 WT mice for 1 h at 4°C to reduce nonspecific binding in samples from APAP-treated mice. The levels of calnexin and GAPDH were also determined as loading controls for microsomes and cytosol, respectively, using rabbit anti-human calnexin and goat anti-rabbit GAPDH (GenScript, Piscataway, NJ). Incubation with these latter antibodies was performed after stripping of the anti-APAP antibody from the blots, through incubation of the blots with a stripping buffer (62.5 mM Tris-HCl, pH 6.8, 2% SDS, and 100 mM β-mercaptoethanol) at 50°C for 30 min.

Determination of Microsomal APAP Metabolism. Metabolic activation of APAP was assayed by a determination of the rates of formation of APAP-GSH adduct; APAP-GSH was measured by use of HPLC with UV detection, as described previously (Gu et al., 1998). Reaction mixtures contained 100 mM potassium phosphate buffer, pH 7.6, 0.5 mM APAP, 0.5 mg/ml microsomal protein, 10 mM GSH, and 1 mM NADPH in a final volume of 0.2 ml. Reactions were carried out at 37°C for 10 min for liver and olfactory mucosa or for 30 min for LNG.

For determinations of the ability of LNG cytosol preparation or ABP to inhibit APAP-GSH formation, increasing amounts of LNG cytosolic protein (0–3 mg/ml) or partially purified mouse ABP (0–32 μg/ml) were added to reaction mixtures containing olfactory mucosa microsomes. Boiled LNG cytosol preparation or boiled ABP was included as negative controls. Mouse ABP was purified from the pooled saliva of ~70-day-old WT B6 male mice, according to a protocol described previously (Karn and Russell, 1993), with a yield estimated to be at least 90%. Aliquots of the various reaction mixtures were also analyzed on immunoblots for detection of APAP-protein adducts, as described above; the reactions were stopped by the addition of >2 volumes of the sample loading buffer for SDS-polyacrylamide gel electrophoresis, followed by immediate heat denaturation of the proteins.

Other Methods. Serum and LNG testosterone levels were determined as described previously (Zhou et al., 2009). Serum (obtained through cardiac puncture) and tissues from individual mice were used for testosterone determination. Metabolism of testosterone was assayed essentially as described previously (Zhou et al., 2009). Quantitative analysis of testosterone metabolites was carried out using LC-MS; the retention times for 15β-hydroxytestosterone, 15α-hydroxytestosterone, 2β-hydroxytestosterone, and 16α-hydroxytestosterone were 10.0, 11.7, 15.1, and 21.5 min, respectively. For determination of the rates of testosterone disappearance, 10 nM testosterone was used, and the reactions were carried out for up to 15 min; the rates were linear with time under this condition. As internal standard, 1 ng of 1,2-D_2-testosterone was added to each sample after termination of the enzyme reaction. For electrophoretic analysis of the purified ABP protein, samples were resolved on a SDS-polyacrylamide gel under reducing conditions (Laemmli, 1970), and the gel was stained with silver by using the PlusOne Silver Staining Kit (GE Healthcare, Chalfont St. Giles, Buckinghamshire, UK). A prestained protein marker (Precision Plus Protein Standards; Bio-Rad Laboratories, Hercules, CA) was used for size determination for silver-stained gels and for immunoblots.

Results

***Cyp2a5*-Null, but not *Cyp2g1*-Null, Mice Are Resistant to APAP Toxicity in the LNG.** To determine the ability of CYP2G1 and CYP2A5 to influence APAP toxicity in the LNG, we compared APAP toxicity in WT B6, *Cyp2a5*-null, and *Cyp2g1*-null male mice. Male mice were studied because the original finding of an increased LNG resistance to APAP toxicity was made with male *Cyp2g1*-null/*Cyp2a5*-low mice (Zhuo et al., 2004). The production and initial characterization of the *Cyp2a5*-null mouse have been reported elsewhere (Zhou et al., 2010), whereas the *Cyp2g1*-null mouse has not been described previously. We used the same gene targeting strategy for the production of the *Cyp2g1*-null mouse as was used previously for the production of the *Cyp2g1*-null/*Cyp2a5*-low mouse (Zhuo et al., 2004), except that the neomycin-resistance (neo) gene, which was used to replace the *Cyp2g1* exon 3 and was presumably responsible for the suppression of the neighboring *Cyp2a5* gene in the *Cyp2g1*-null/*Cyp2a5*-low mouse, was removed in the *Cyp2g1*-null mouse through Cre-mediated recombination in zygotes.

The structures of the WT *Cyp2g1* allele, the targeting construct, the *Cyp2g1*-null allele with a floxed neo inserted, and the *Cyp2g1*-null allele without neo are shown in Fig. 1A. The structural integrity of the targeted *Cyp2g1* allele and the absence of random integration of the targeting construct were confirmed by Southern blot analysis using both internal and external probes (data not shown). Absence of *Cyp2g1* expression in the *Cyp2g1*-null mice was confirmed by PCR analysis of CYP2G1 mRNA in the olfactory mucosa of both male and female mice (Fig. 1B). The normal CYP2A5 expression in the *Cyp2g1*-null mice confirms our previous hypothesis that the lowered CYP2A5 expression seen in the original *Cyp2g1*-null/*Cyp2a5*-low mouse was due to the presence of neo at the *Cyp2g1* exon 3 (Zhuo et al., 2004) and was validated by immunoblot analysis of CYP2A5 protein in the olfactory mucosa, LNG, and liver (Fig. 1C).

The *Cyp2a5*-null mice and the *Cyp2g1*-null mice, which were both produced by using ES cells derived from the B6 strain, are maintained on a B6 genetic background. Both models exhibited normal growth rates and reproductive ability and no structural abnormality was found in their olfactory mucosa and LNG upon histological analysis (data not shown). The *Cyp2g1*-null, *Cyp2a5*-null, and WT B6 male mice were then used for APAP toxicity studies. As shown in Fig. 2, the LNG of both WT (A and D) and *Cyp2g1*-null mice

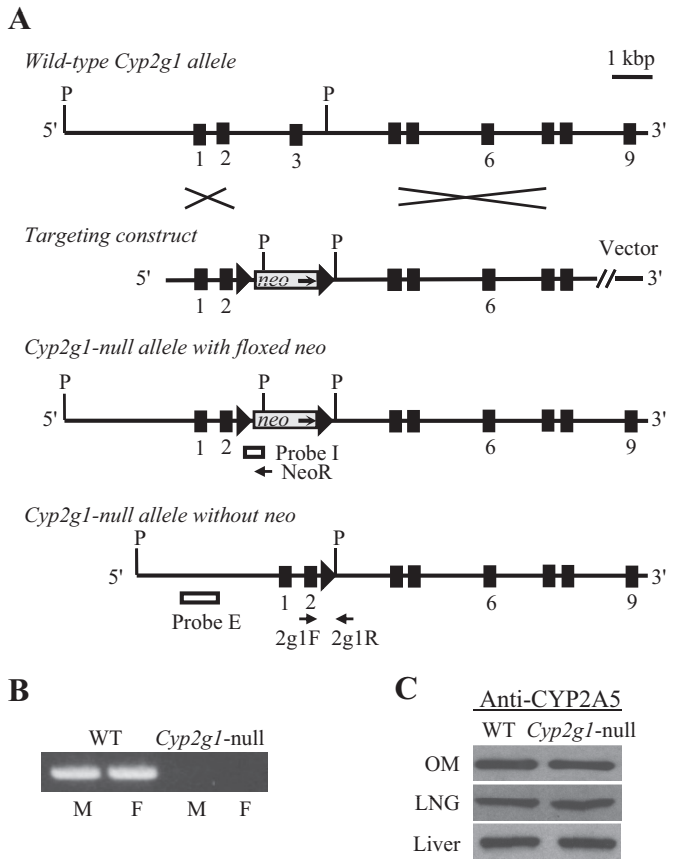

Fig. 1. Targeted disruption of the mouse *Cyp2g1* gene. A, structures of the WT *Cyp2g1* allele, the targeting vector, the *Cyp2g1* allele with a floxed neo insertion, and the *Cyp2g1* allele without neo. Positions of the PCR primers (2g1F, 2g1R, and NeoR) used for genotyping, as well as the Pst I restriction sites (P) and the external (Probe E) and internal (Probe I) probes used for Southern blot analysis, are indicated. Triangles represent loxP sites; selected exons are numbered below. B, absence of CYP2G1 expression in the *Cyp2g1*-null mice. RNA-PCR was performed using total RNA prepared from the olfactory mucosa of adult male (M) or female (F) WT B6 or *Cyp2g1*-null mice. PCR products were analyzed on an agarose gel and visualized by staining with ethidium bromide. C, normal CYP2A5 expression in the *Cyp2g1*-null mice. Immunoblot analysis was performed for microsomal proteins (5 μg per lane for LNG and 1 μg per lane for olfactory mucosa and liver) of the WT B6 and *Cyp2g1*-null mice, with use of an anti-CYP2A5 antibody. Microsomes were prepared from pooled olfactory mucosa, LNG, or liver from five male mice (2 months old). Densitometric analysis (not shown) indicated that the maximal difference in band intensity between samples from WT and the *Cyp2g1*-null groups was less than 10%. Typical results are shown.

(B and E) was severely damaged at 24 h after a single injection of APAP (400 mg/kg i.p.), resulting in extensive tissue necrosis, as described previously for APAP-treated WT B6 or 129/Sv mice (Zhuo et al., 2004). In contrast, the LNG of APAP-treated *Cyp2a5*-null mice was intact (C and F), which indicated that CYP2A5, but not CYP2G1, influences APAP toxicity in the LNG. This finding ruled out the previously proposed possibility that CYP2G1, which is located only in the olfactory mucosa, can act through a paracrine pathway to indirectly influence resistance of the LNG to chemical toxicity (Zhuo et al., 2004).

The resistance of the *Cyp2a5*-null mice to APAP-induced LNG toxicity was also evident in experiments that measured tissue levels of total nonprotein thiols in the LNG. As shown in Table 1, at 2 h after APAP treatment, LNG total nonprotein thiol levels were decreased by 69% in WT B6 mice but were unchanged in the *Cyp2a5*-null mice compared with saline-treated mice. For a comparison, substantial (86–87%) decreases in total nonprotein thiol levels were observed in the livers of both WT and *Cyp2a5*-null mice, thus documenting tissue-specific protection of the LNG against APAP toxicity in the *Cyp2a5*-null mice.

The *Cyp2a5*-Null Mouse Does Not Show Alterations in Rates of APAP Metabolic Activation in the LNG or in Systemic APAP Clearance, but It Does Show Decreased APAP and APAP-GSH Levels in the LNG. In efforts to identify the mechanisms underlying the observed resistance of the LNG against APAP toxicity in the *Cyp2a5*-null mice, we sought to determine whether the *Cyp2a5*-null mice had decreased rates of APAP metabolic activation in the target tissue or in the liver or else somehow had decreased circulating levels of APAP. In vitro studies using microsomes prepared from the liver and LNG of WT and *Cyp2a5*-null male mice indicated that the rates of APAP metabolic activation, measured by the rates of formation of APAP-GSH, were not different in the two mouse strain, for either liver or LNG (Table 2). This result, which was consistent with previous findings of an unaltered metabolic activation of APAP in the LNG of *Cyp2g1*-null/*Cyp2a5*-low mice (Zhuo et al., 2004), confirmed that the resistance seen in the *Cyp2a5*-null mice was not due to a decrease in rates of target tissue metabolic activation in the LNG or to a decrease in APAP metabolic activation in the liver. In this connection, immunoblot analysis revealed that, in addition to CYP2A5, the enzymes CYP2E1 and CYP3A, which are also capable of activating APAP (Patten et al., 1993), are expressed in the LNG; the LNG expression levels of these latter enzymes, as well as that of the P450 reductase, were not different between the WT and *Cyp2a5*-null mice (data not shown).

The levels of APAP and APAP-GSH in the plasma and

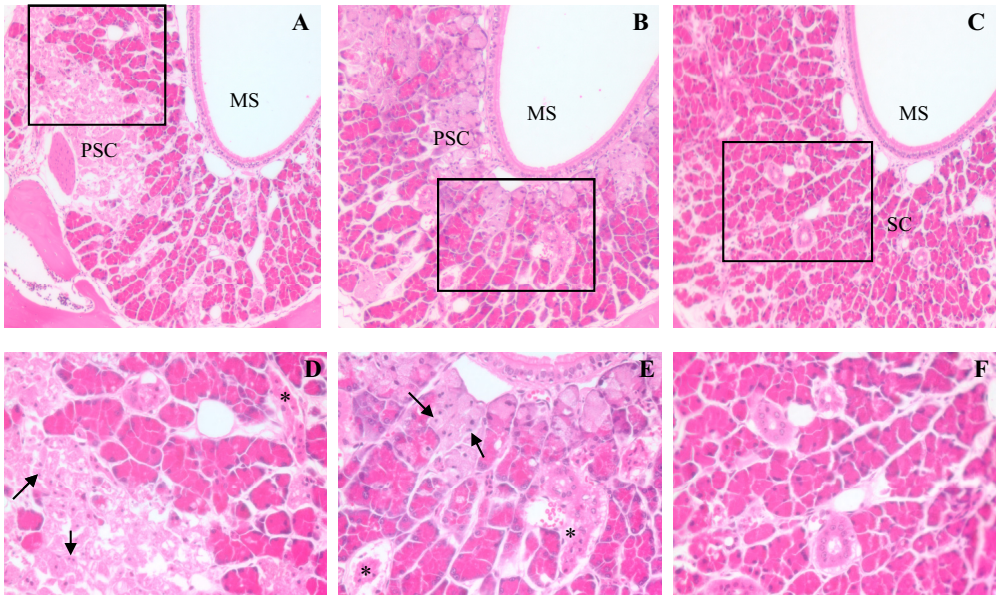

Fig. 2. Histological analysis of APAP toxicity in the LNG. Male, 2-month-old B6 WT, *Cyp2g1*-null, and *Cyp2a5*-null mice (eight in each group) were treated, at 9:00 to 10:00 AM after overnight fasting, with a single injection of APAP (400 mg/kg i.p.) in warm saline. Control groups (not shown) received the vehicle only. Mice were killed at 24 h after the APAP injection. All sections were at the level of the second palatal ridge (level 5 in Young, 1981). Typical images are shown, at either 100× (A–C) or 400× (D–F, for boxed area only) magnification. LNG in APAP-treated WT (A) and *Cyp2g1*-null (B) mice exhibited extensive cell necrosis, as indicated by the widespread appearance of pale, ragged secretory cells (PSC) and dark, shrunken duct cells (*), and apoptotic glandular epithelial cells (arrows); LNG in APAP-treated *Cyp2a5*-null mouse (C) had normal, palely staining duct cells with open face nuclei and plump secretary cells (SC) with bright eosinophilic cytoplasmic granules. MS, maxillary sinus.

TABLE 1

Effects of APAP treatment on the levels of total nonprotein thiols in the liver and the LNG

Two- to 3-month-old male WT B6 and *Cyp2a5*-null mice were fasted overnight before a single injection of APAP (400 mg/kg i.p.) in saline or of saline alone. Tissues were dissected from individual mice at 2 h after APAP injection. The values shown represent means ± S.D.

Tissue & Treatment	WT		*Cyp2a5*-Null	
	Total Nonprotein Thiols	APAP/Saline	Total Nonprotein Thiols	APAP/Saline
	μmol/g tissue	%	*μmol/g tissue*	%
LNG (n = 4)				
Saline	1.02 ± 0.06		0.97 ± 0.12	
APAP	0.32 ± 0.03[a]	31.3	0.90 ± 0.02	92.7
Liver (n = 8)				
Saline	6.35 ± 0.85		6.20 ± 0.45	
APAP	0.91 ± 0.08[a]	14.3	0.82 ± 0.07[a]	13.2

[a] $P < 0.01$, APAP versus saline for a given tissue of the same mouse strain.

LNG were examined at various times after dosing, to determine whether circulating or target-tissue bioavailability of APAP was by some means decreased in the *Cyp2a5*-null mouse, leading to decreased LNG toxicity. Plasma APAP (Fig. 3A) or APAP-GSH (Fig. 3C) levels were not different in WT and *Cyp2a5*-null mice at any of the three time points examined; plasma levels of major phase II metabolites of APAP (APAP-S, formed by sulfotransferase, and APAP-G, formed by UDP-glucuronosyltransferase) were also not different in the two mouse strains (Fig. 3E, 3G). However, LNG APAP (Fig. 3B) and APAP-GSH (Fig. 3D) levels were reduced at all three time points, by ~40 and 50%, respectively, at 2 h after dosing in the *Cyp2a5*-null mice compared with the WT mice, whereas APAP-S and APAP-G levels in the LNG were not different in WT and *Cyp2a5*-null mice at any of the time points examined (Fig. 3, F and H). Taken together, these results indicate that, although the disruption to *Cyp2a5* caused no changes in rates of APAP metabolic activation in the LNG or changes in the rates of systemic APAP clearance, it did lead to a sizable decrease in the tissue burdens of APAP and APAP-GSH in the LNG.

It is noteworthy that APAP-G was the predominant metabolite in the circulation, whereas APAP-S and APAP-GSH were detected at much lower abundance (Fig. 3). The levels of APAP-G and APAP-S in the LNG were ~1/10 of that in the plasma, whereas the levels of APAP were approximately the same as those in the plasma; this discrepancy may reflect differential abilities of APAP and its conjugated metabolites to distribute from the blood to tissues, as well as lower extents of conjugation of APAP via the -GSH, -S, and -G pathways in the LNG compared with the extents in other tissues that contribute to plasma levels of these AP metabolites.

The levels of APAP-GSH in the LNG were also lower than those in the plasma. However, the time course for the changes in plasma levels differed in APAP and APAP-GSH; whereas APAP levels were maximal at 15 min after injection (the first time point monitored) and decreased thereafter, the APAP-GSH levels peaked at 60 min. Intriguingly, a similar divergence in the apparent T_{max} values was not observed for APAP and APAP-GSH levels in the LNG, where both APAP and APAP-GSH levels were highest at 15 min after dosing. Possible explanations for the difference in the apparent T_{max} of APAP-GSH in plasma and in LNG may include an increased mucus secretion from the LNG upon exposure to APAP and a lag in the further degradation of the APAP-GSH by peptidases in the LNG in both WT and *Cyp2a5*-null mice.

Up-Regulation of ABP Expression in the LNG of the *Cyp2g1*-Null/*Cyp2a5*-Low and *Cyp2a5*-Null Mice. Decreases in the levels of LNG APAP (a substrate for local

TABLE 2

In vitro metabolism of APAP by liver and LNG microsomes from WT and *Cyp2a5*-null mice

Rates of formation of the major in vitro APAP metabolite, APAP-GSH, were determined. Reaction mixtures contained 100 mM potassium phosphate buffer, pH 7.6, 0.5 mM APAP, 10 mM GSH, 0.5 mg/ml liver or LNG microsomal protein from 2-month-old male mice, and 1.0 mM NADPH. The values presented are means ± S.D. (n = 3).

Strain	Rates of APAP-GSH Formation	
	Liver	LNG
	nmol · min^{-1} *· mg protein*$^{-1}$	
WT	0.46 ± 0.04	0.08 ± 0.01
Cyp2a5-null	0.43 ± 0.02	0.07 ± 0.01

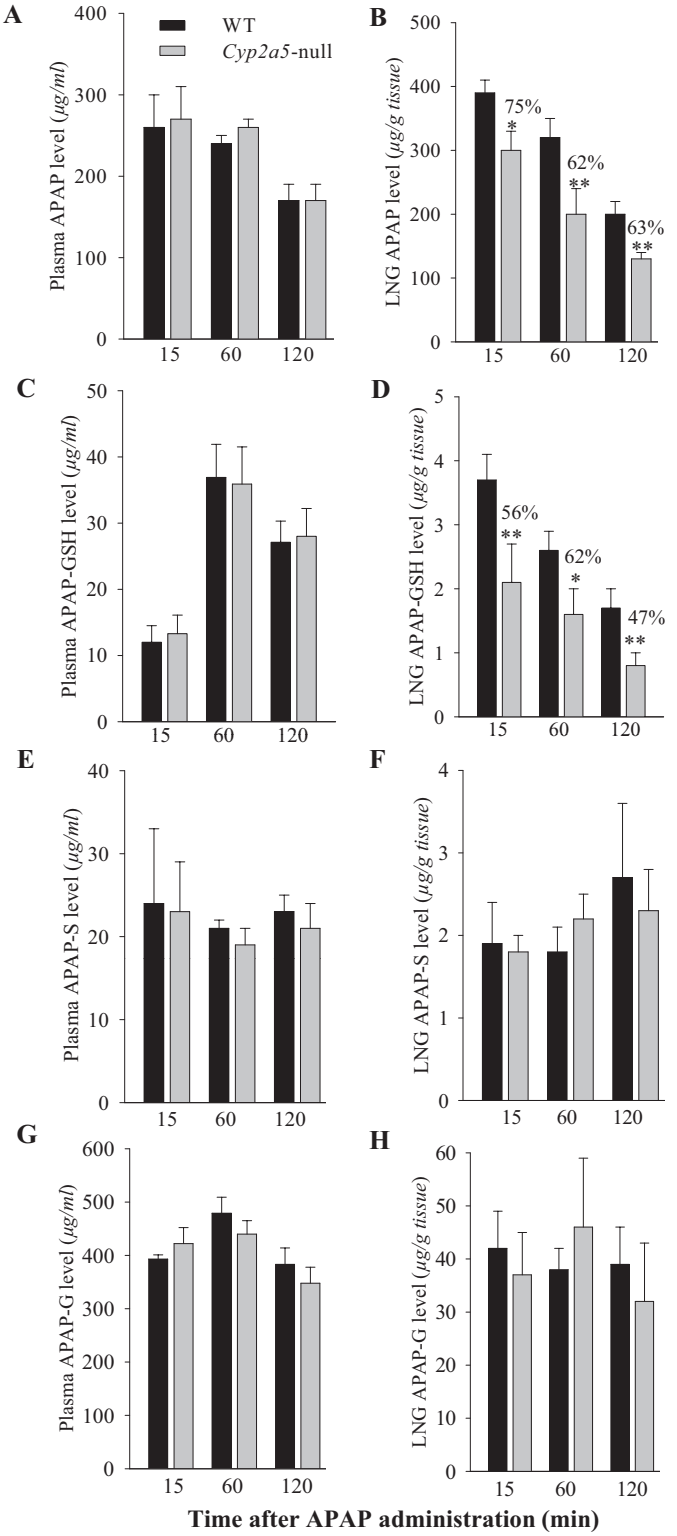

Fig. 3. Levels of APAP, APAP-GSH, APAP-S, and APAP-G in the plasma and LNG of WT and *Cyp2a5*-null mice at various times after APAP treatment. Two- to 3-month-old male mice, either B6 WT or *Cyp2a5*-null, were fasted overnight before a single injection of APAP (400 mg/kg i.p.). LNG and plasma were obtained from treated mice at 15 min, 1 h, or 2 h after APAP injection for determination of APAP (A and B; $n = 6$), APAP-GSH (C and D; $n = 4$), APAP-S (E and F; $n = 4$), and APAP-G (G and H; $n = 4$) levels. Values represent means ± S.D. **, $P < 0.01$; *, $P < 0.05$, Student's t test, for comparisons between WT and *Cyp2a5*-null mice.

metabolic activation) and APAP-GSH [potentially involved in the GSH depletion through the γ-glutamyl cycle, as suggested by our previous finding that APAP toxicity in the LNG is significantly influenced by APAP metabolic activation in the liver (Gu et al., 2005)] could both contribute to decreased APAP toxicity in that tissue. However, the relatively small extents of the observed decreases suggested that the mechanisms underlying the resistance of *Cyp2a5*-null mouse to APAP toxicity involve additional molecular events beyond the metabolic activation step. In that connection, we had performed a microarray analysis of gene expression differences between the LNG of the *Cyp2g1*-null/*Cyp2a5*-low male mice (on mixed B6 and 129/Sv genetic background) and the LNG of the WT B6 or 129/Sv male mice. This identified two genes encoding subunits of the complex androgen-binding protein system. These are *Abpa27* and *Abpbg27*, the products of which form a disulfide-bridged dimeric protein described previously in mouse salivary glands and saliva (Dlouhy et al., 1987; Laukaitis et al., 2008 and references therein). These two genes are among those that had the greatest up-regulation in the *Cyp2g1*-null/*Cyp2a5*-low mice compared with mice of either WT strain (Table 3). The up-regulation of both ABP mRNA and protein expression was confirmed by quantitative RNA-PCR and by immunoblot analysis, respectively, in the *Cyp2g1*-null/*Cyp2a5*-low mice (not shown) and in the *Cyp2a5*-null mice (Fig. 4). In the *Cyp2a5*-null mouse, mRNA levels for *Abpa27*, encoding a major ABP α subunit detected in the LNG (Zhou et al., 2009), were ~3-fold higher than in WT B6 mice (Fig. 4A), and the levels of ABP protein in the cytosol preparation were also ~3-fold higher (Fig. 4B). The cytosolic localization of ABP protein was confirmed by immunoblot analysis of various subcellular fractions (Fig. 4C).

As shown in Table 3, the expression of lipocalin-type prostaglandin D_2 synthase was also highly up-regulated in the *Cyp2g1*-null/*Cyp2a5*-low mice; this up-regulation was subsequently confirmed at both mRNA and protein levels for the *Cyp2g1*-null/*Cyp2a5*-low mice, but not for the *Cyp2a5*-null mice (data not shown). The disparate results from the two mouse strains indicate that lipocalin-type prostaglandin D_2 synthase is not relevant to the resistance to APAP toxicity in the *Cyp2g1*-null/*Cyp2a5*-low or the *Cyp2a5*-null mice. The potential roles in the altered resistance to APAP toxicity of the other genes that were found to be up- or down-regulated in the LNG of the *Cyp2g1*-null/*Cyp2a5*-low mice (Table 3) have not been examined. It is noteworthy that although ABCC5 (MRP5), an organic anion transporter capable of transporting GSH conjugates such as *S*-(2, 4-dinitrophenyl)-GSH (Wijnholds et al., 2000), seemed to be up-regulated (Table 3), its signal intensity on the gene array was quite low, and the corresponding protein was not detected in the LNG by immunoblot analysis (data not shown).

Impact of *Cyp2a5* Deletion on Testosterone Metabolism and Homeostasis in the LNG. Our recent finding that the LNG of male mice contains unusually high levels of testosterone together with the known ability of CYP2A5 to metabolize testosterone prompted us to examine testosterone levels in the LNG of the *Cyp2a5*-null mice. It is noteworthy that although recombinant CYP2A5 can metabolize testosterone (Gu et al., 1999), the loss of CYP2A5 expression did not lead to a large decrease in the overall rates of testosterone metabolism by hepatic microsomes in vitro or a significant change in circulating levels of testosterone in vivo (Zhou et al., 2010). As shown in Table 4, in the LNG of the *Cyp2a5*-null mice, in vitro microsomal testosterone hydroxylase activities in the formation of the most abundant metabolite, 15α-hydroxytestosterone, and two minor products, 15β-hydroxytestosterone and 2β-hydroxytestosterone (all known metabolites by CYP2A5), were essentially abolished, whereas the rates of formation of another minor product, 16α-hydroxytestosterone, were unchanged, with testosterone

TABLE 3

Genes that were differentially expressed in the LNG of *Cyp2g1-null*/*Cyp2a5*-low and WT mice

RNA from 2-month-old male mice was used for microarray analysis, with use of the Affymetrix Mouse Expression Set 430A GeneChip arrays. LNGs from 10 mice were pooled for the preparation of each RNA sample, and a total of nine LNG RNA samples were analyzed (four from B6 WT, two from WT 129/Sv, and three from *Cyp2g1-null*/*Cyp2a5*-low). Genes with significantly changed expression ($P < 0.05$), and with change values either greater than 1.5-fold or smaller than 0.67-fold in comparisons of both *Cyp2g1*-null/*Cyp2a5*-low with B6 and *Cyp2g1*-null/*Cyp2a5*-low with 129/Sv in at least one probe set, are shown. Probe sets for which none of the three groups had averaged expression values greater than 60 (after GC-RMA normalization) were excluded.

Gene Symbol	Change		Gene Name
	Cyp2g1-Null/*Cyp2a5*-Low:129/Sv	*Cyp2g1*-Null/*Cyp2a5*-low:B6	
	fold		
Ptgds	7.67/12.39	8.72/12.37	L-type prostaglandin D2 synthase
Abpa	7.45	1.75	Androgen binding protein, α[a]
Abpb	6.18	2.05	Androgen binding protein, β[b]
S100a10	2.70	1.68	S100 calcium binding protein A10
Sdc4	2.25	4.78	Syndecan 4
Cebpd	1.90	1.62	CCAAT/enhancer binding protein, delta
Abp1	1.71	2.01	Amiloride binding protein 1
Calml4	1.70	1.91	Calmodulin-like 4
Ramp1	1.66	1.56	Receptor activity modifying protein
Foxa1	1.62	1.69	Forkhead box A1
Thbs1	1.57	1.66	Thrombospondin 1
Abcc5	1.57	1.59	ATP binding cassette, subfamily C, member 5
Ccl28	1.54/1.69	1.68/1.52	C-C motif ligand 28
Igfbp5	1.53	1.69	Insulin-like growth factor binding protein 1
D6WSU176e	0.63	0.65	DNA segment Chr6, Wayne State Univ. 176, expressed
Pnliprp1	0.62	0.51	Pancreatic lipase-related protein 1
Dhrs	0.56	0.58	Dehydrogenase/reductase, member 7
Adh1	0.53	0.33	Alcohol dehydrogenase 1
Cyp2a5	0.02	0.03	Cytochrome P450, 2A5

[a] The probes used are common for a number of *Abpa* genes, including *Abpa27*.
[b] The probes used are common for a number of *Abpb* genes, including *Abpbg27*.

at 10 μM. The overall rates of testosterone disappearance were also substantially decreased (with testosterone at 10 nM) in the LNG of *Cyp2a5*-null mice (Table 4). Furthermore, LNG testosterone levels were ~2.5-fold higher in the *Cyp2a5*-null than in WT male mice, whereas serum testosterone levels were comparable in the two groups (Fig. 5, A and B). Large variations among individual mice were noted in both serum and LNG testosterone levels. A correlation analysis indicated that, within each strain, the variations in the LNG were highly correlated with variations in the serum (Fig. 5C), a result consistent with the notion that LNG testosterone is derived from the circulation (Zhou et al., 2009) and that rates of local metabolism influence tissue testosterone levels. In experiments not shown, substantial decreases in LNG microsomal testosterone metabolism and significant increases in LNG testosterone levels were also observed in male *Cyp2g1*-null/*Cyp2a5*-low mice. Taken together, these findings indicate that CYP2A5 plays a critical role in the maintenance of testosterone homeostasis in a tissue-specific fashion in the LNG of male mice.

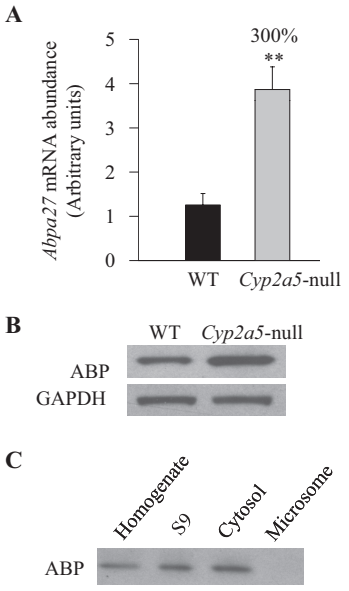

Fig. 4. ABP expression in the LNG of WT and *Cyp2a5*-null mice. A, quantitative RNA-PCR analysis of Abpa27 mRNA expression in B6 WT and *Cyp2a5*-null mice. LNGs from individual 2- to 3-month-old male mice were used for total RNA preparation. The relative levels of Abpa27 in LNG were determined. The results were corrected on the basis of the levels of GAPDH mRNA present in the same preparation. Data represent means ± S.D. ($n = 4$); **, $P < 0.01$, Student's t test, for comparisons between WT and *Cyp2a5*-null mice. B, immunoblot analysis of ABP protein levels in the LNG cytosol preparation from B6 WT and *Cyp2a5*-null mice. Cytosol fractions were prepared from pooled LNGs from 10 2- to 3-month-old male WT or *Cyp2a5*-null mice. Levels of GAPDH protein were also determined as a loading control. Samples (40 μg of protein per lane) were analyzed with use of either an anti-ABP antibody or an anti-GAPDH antibody. Densitometric analysis (not shown) indicated a ~3-fold higher level of ABP expression in the *Cyp2a5*-null than in WT LNG. C, immunoblot analysis of ABP protein expression in subcellular fractions of the WT LNG. Pooled LNGs from 10 2- to 3-month-old male B6 WT mice were used for the preparation of tissue homogenate, postmitochondrial S9 fraction (S9), cytosol, and microsome fractions. For immunoblot analysis, 40 μg of protein were analyzed per lane.

Correlation between ABP and Testosterone Levels in the LNG of the *Cyp2a5*-Null Mice. ABP has been shown to bind testosterone, progesterone, and dihydrotestosterone (Karn, 1998). We wished to test the possibility that ABP expression in the LNG is under feedback regulation by testosterone. We performed correlation analysis of serum testosterone levels and LNG ABP protein levels in a group of WT male mice. Both parameters showed wide interanimal variations (Fig. 5D), yet they were strongly correlated with each other, with an r value of 0.883 ($p < 0.05$). Thus, it seems possible that the increased abundance of testosterone led to the augmented ABP expression in the LNG of the *Cyp2a5*-null mice.

Ability of ABP to Compete with GSH and Cellular Proteins for Adduction with Reactive Metabolites of APAP In Vitro. The mature, secreted form of ABP is a heterodimer composed of an α and a βγ subunit disulfide-bridged in antiparallel configuration involving Cys3 and Cys69 (Karn and Laukaitis, 2003). Each subunit contains a third cysteine whose sulfhydryl status has yet to be determined. Given the known ability of reactive APAP metabolites to attack sulfhydryl groups in proteins, and the abundance of the cysteine-containing ABP (Zhou et al., 2009), we speculate that the sulfhydryl groups of the ABP subunits could be a major target for adduction by reactive APAP metabolites either before ABP dimers can be formed or upon dissociation of the heterodimers into subunits. Therefore, an increase in ABP subunit levels in the LNG, as was found in the *Cyp2a5*-null mouse (Fig. 4), would serve to shield other cellular proteins and thiol groups against adduction by APAP metabolites. To test this hypothesis, we first compared the ability of LNG cytosol preparation from WT mice with that from *Cyp2a5*-null mice to inhibit APAP-GSH formation in vitro, in reaction mixtures containing mouse olfactory mucosa microsomes (as a rich source of CYP2A5), APAP, NADPH, and GSH. As shown in Fig. 6A, addition of LNG cytosol preparation caused concentration-dependent inhibition of APAP-GSH formation, the LNG cytosol preparation from *Cyp2a5*-null mice being significantly more effective. This result is consistent with the idea that the greater abundance of ABP in the LNG of the *Cyp2a5*-null mice can lead to greater inhibition of APAP-GSH formation.

TABLE 4

In vitro metabolism of testosterone by LNG microsomes from WT and *Cyp2a5*-null mice

Rates of formation of 15α-OH-T, 15β-OH-T, 2β-OH-T, and 16α-OH-T, as well as the rates of disappearance of testosterone, in microsomal incubations, were determined. Reaction mixtures contained 50 mM potassium phosphate buffer, pH 7.4, 10 μM (for metabolite formation) or 10 nM (for substrate disappearance) testosterone, 1.0 mM ascorbic acid, 0.5 mg/ml LNG microsomal protein from 2-month-old male mice, and 1.0 mM NADPH. The values presented are means ± S.D. ($n = 3$).

Strain	Rates of Product Formation				Rates of Testosterone Disappearance
	15α-OH-T	15β-OH-T	2β-OH-T	16α-OH-T	
			pmol · min⁻¹ · mg protein⁻¹		
WT B6	106 ± 19	7.8 ± 1.6	8.8 ± 2.5	12.0 ± 2.0	0.7 ± 0.03
Cyp2a5-null	0.3 ± 0.1[a]	< 0.04[a]	< 0.4[a]	11.7 ± 1.5	0.3 ± 0.02[a]

OH-T, hydroxytestosterone.
[a] $P < 0.01$ compared with the corresponding value of WT mice.

However, more direct evidence was needed to demonstrate the ability of ABP to form APAP adducts. We next added ABP prepared from mouse saliva to reaction mixtures containing olfactory mucosa microsomes, APAP, NADPH, and GSH. The preparation of partially purified ABP exhibited a cluster of partially resolved, prominent bands in the 10-kDa region (which corresponded well with the position of ABP subunits detected by immunoblot analysis, and presumably represents a mix of the α and β subunits of various ABP isoforms), as well as a few minor bands (not recognized by the anti-ABP antibody) in higher molecular weight regions upon electrophoretic analysis (under reducing conditions) and silver staining (Fig. 6B). Addition of the ABP preparation caused concentration-dependent inhibition of APAP-GSH formation (Fig. 6C). As was found for boiled LNG cytosolic proteins, boiled ABP was incapable of inhibiting APAP-GSH formation. This finding suggests that heat denaturation will make the sulfhydryl groups in ABP and other cytosolic proteins inaccessible to the reactive APAP metabolites.

In Fig. 6C, the highest concentration of salivary ABP used was ~33 μg/ml (~1.65 μM), which was much lower than the levels of APAP (0.5 mM) added to the assays but not too far from the amounts of APAP-GSH that were blocked from formation (~10 μM), if we consider the possible involvement of multiple Cys residues of each ABP subunit as targets for APAP adduction. Thus, the inhibitory effect is more than can be explained by noncovalent binding of APAP to the ABP heterodimer. The inhibitory effect was also not due to a direct inhibition of the formation of the reactive intermediate, because the inhibitory effects can be overcome by addition of greater amounts of GSH (data not shown).

Addition of salivary ABP to reactions without GSH led to time-dependent formation of a unique APAP adduct, detected by an antibody to APAP (Fig. 6D). We believe that this represents an adduct of APAP with an ABP subunit (APAP-ABP) on the basis of its migration rate, identical to that of ABP subunits on immunoblot, as well as its detection by both anti-APAP and anti-ABP and its increases in abundance with the increases in the amounts of ABP added (Fig. 6E). As further controls, formation of the APAP-ABP adduct was nearly abolished by the addition of an excess amount (10 mM) of GSH (Fig. 6D) or when either APAP or NADPH was omitted (data not shown). In addition, APAP-ABP and other APAP-protein adducts were detected when LNG cytosol preparation was added to olfactory mucosa microsomal reactions with APAP (Fig. 6E); notably, few APAP adducts with microsomal proteins were detected, most likely because of the relatively low amounts of total microsomal protein used in the assay. It is noteworthy that addition of salivary ABP to reactions containing LNG cytosol preparation led to increases in the abundance of APAP-ABP, and decreases in the abundance of the other APAP-protein adducts. This result is consistent with the ability of ABP subunits to compete with cellular proteins for binding to reactive APAP metabolites.

The inhibitory effects of ABP addition on APAP-GSH formation (Fig. 6C) and on APAP-protein adduct formation (Fig.

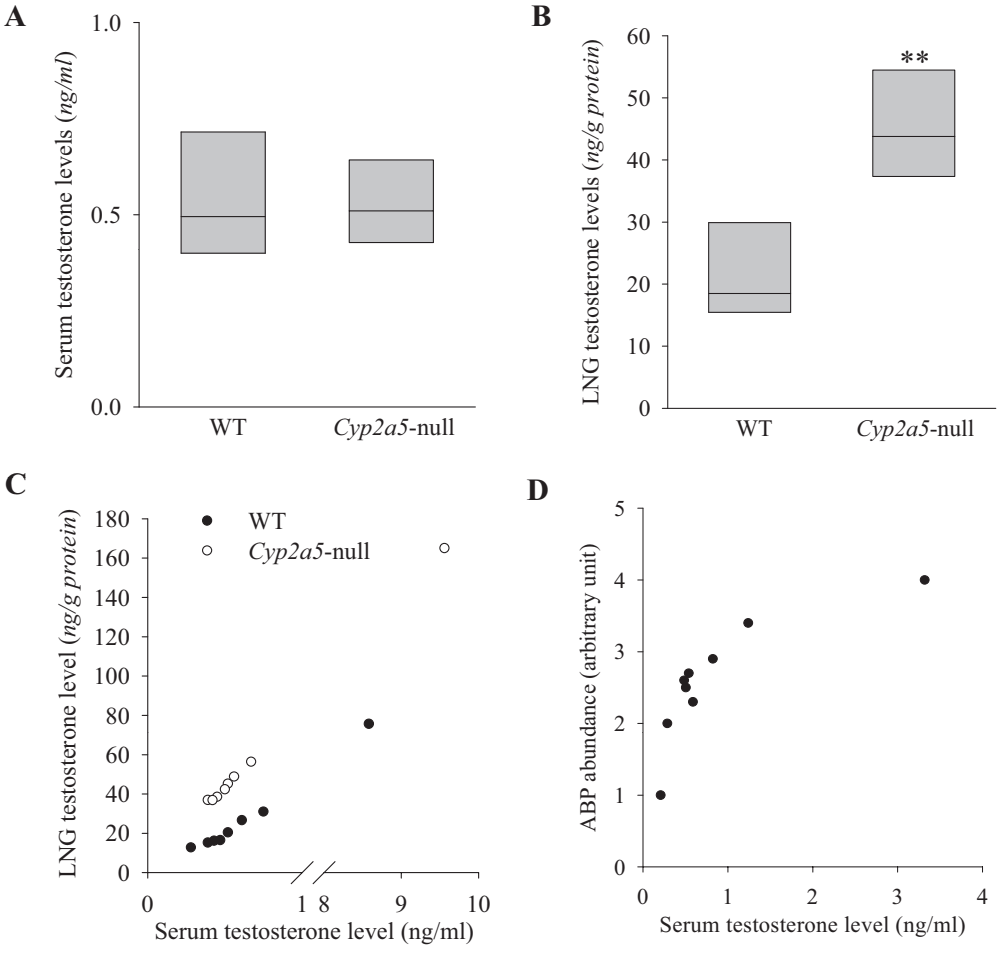

Fig. 5. Testosterone levels in the serum and LNG of WT and *Cyp2a5*-null male mice. Serum (A) and LNG (B) testosterone levels were determined for 2- to 3-month-old male B6 WT and *Cyp2a5*-null mouse. The values shown are the medians, together with the 25% (lower bar) and 75% (upper bar) percentile marks. Testosterone levels in the LNG (but not the levels in the serum) were significantly higher in the *Cyp2a5*-null than in the WT mice ($n = 8$); **, $P < 0.01$, Mann-Whitney rank sum test. C, correlation of LNG testosterone levels with serum testosterone levels. LNG and serum testosterone levels for each mouse were plotted. The correlation coefficient (r) for LNG versus serum is 1.000 ($P < 0.01$) in WT, and 0.976 in *Cyp2a5*-null ($P < 0.01$) mice; Spearman rank order correlation test. D, correlation of LNG ABP protein levels with serum testosterone levels. LNG cytosol ABP levels determined by immunoblot analysis and serum testosterone levels were determined for nine male B6 mouse (2- to 3-month old). The correlation coefficient (r) for LNG ABP versus serum is 0.883 ($P < 0.05$); Spearman rank-order correlation test.

6E) were consistent, except that the blockage of cytosolic protein adduct formation was more complete because of the absence of added GSH. It is noteworthy that because the smaller proteins typically have poorer retention on the nitrocellulose membrane than the larger proteins do during electrophoretic transfer, the intensity of the APAP-ABP band was relatively low (e.g., Fig. 6E, last lane), and it did not match the intensity of the cytosolic protein adducts detected in the higher molecular weight region in the absence of added ABP (Fig. 6E, lane 4).

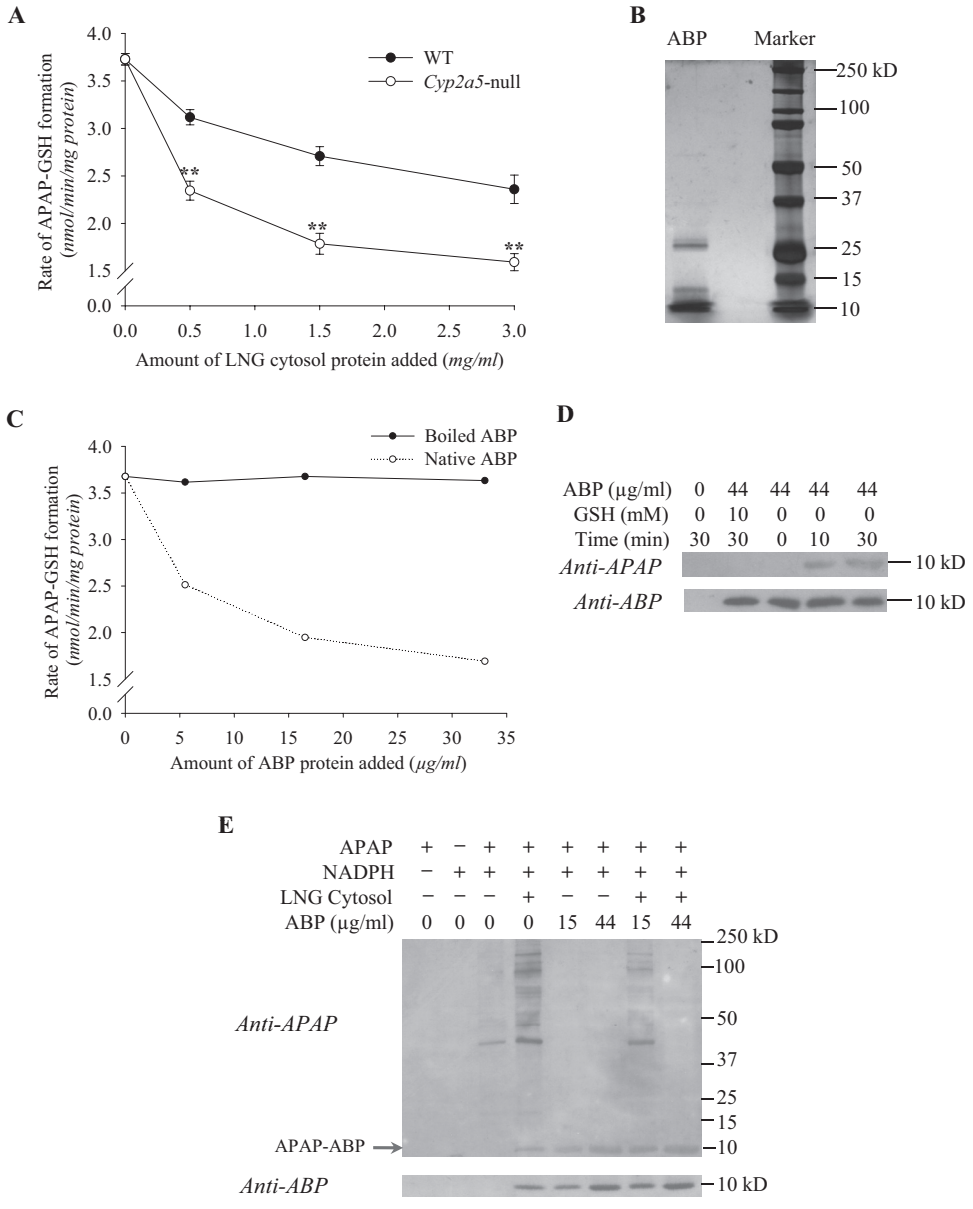

Fig. 6. Ability of ABP to compete with GSH and cellular proteins for adduction with APAP in vitro. Reaction mixtures contained 100 mM potassium phosphate buffer, pH 7.6, 0.5 mM APAP, 0.5 mg/ml olfactory mucosa microsomal protein of 2- to 3-month-old male B6 WT mice, and other components as indicated. Unless otherwise indicated, reactions were carried out for 10 min at 37°C. A, differential inhibition of APAP-GSH formation by LNG cytosol preparation from WT and *Cyp2a5*-null mice. Rates of in vitro formation of APAP-GSH were determined in the presence of 1.0 mM NADPH, 0.2 mM GSH, and increasing amounts of LNG cytosolic protein (0–3 mg/ml), prepared from 2-month-old male WT or *Cyp2a5*-null mice. The values presented are means ± S.D. ($n = 3$); ** $P < 0.01$, Student's t test. In negative control reactions, the addition of boiled LNG cytosol preparation from 2-month-old male WT mice (at 3 mg/ml) did not affect rates of APAP-GSH formation (data not shown). B, gel-electrophoretic analysis and silver staining of partially purified ABP protein. A preparation of ABP (~2 μg of protein) purified from mouse saliva was analyzed under reducing condition on a 10% polyacrylamide gel. Selected fragments of a prestained protein size marker are labeled. C, inhibition of APAP-GSH formation by purified ABP. Rates of formation of APAP-GSH were determined in the presence of 1.0 mM NADPH, 0.2 mM GSH, and increasing amounts of either boiled or native ABP (at 0–33 μg/ml; amounts equivalent to those of ABP present in 0 to 3 mg/ml LNG cytosol protein from *Cyp2a5*-null mice). The values presented are averages for duplicated samples at each ABP concentration. D, time-dependent formation of APAP-ABP protein adduct in vitro. Reactions were carried out for 0 to 30 min in the presence of 1.0 mM NADPH, 0 or 44 μg/ml ABP, and 0 or 10 mM GSH. Aliquots of the reaction mixtures, equivalent to 5 μg of the olfactory mucosa microsomal protein per lane, were analyzed on immunoblots, with use of either an anti-APAP or an anti-ABP. E, Competition between ABP and other LNG cytosolic proteins for adduction with APAP. Reactions were performed as in C, except that LNG cytosol preparation from *Cyp2a5*-null mice was added at 1.5 mg/ml, whereas the concentration of ABP varied between 0 and 44 μg/ml. Addition of ABP to reactions containing LNG cytosol led to increases in the abundance of APAP-ABP, and decreases in the abundance of the other APAP-protein adducts.

Increased Formation of APAP-ABP Protein Adduct, Accompanied by Decreased Formation of APAP Adducts with Other Cellular Proteins, in the LNG of APAP-Treated *Cyp2a5*-Null Mice, Compared with the LNG of APAP-Treated WT Mice. The ability of ABP to form APAP adducts in the LNG in vivo in APAP-treated mice was then examined. As shown in Fig. 7A, after a treatment of the animals with a toxic dose of APAP (400 mg/kg), many bands representing APAP-protein adducts were detected with the anti-APAP antibody in the microsomal or cytosolic fractions of the LNG from WT mice, including a band at ~10 kDa, which was detected in the cytosol preparation both by anti-APAP (Fig. 7A) and by anti-ABP (Fig. 7B). The intensity of the APAP-ABP band was greater (>2-fold; Fig. 7A), whereas the intensities of the other adduct bands in either microsome or cytosol fractions were much reduced, in the LNG of APAP-treated *Cyp2a5*-null mice. These results strongly support the notion that the increased ABP subunit abundance in the *Cyp2a5*-null LNG serves to quench greater amounts of reactive APAP metabolites, thus sparing the other perhaps more critical cellular proteins from adduction by APAP metabolites and protecting the cells against necrosis.

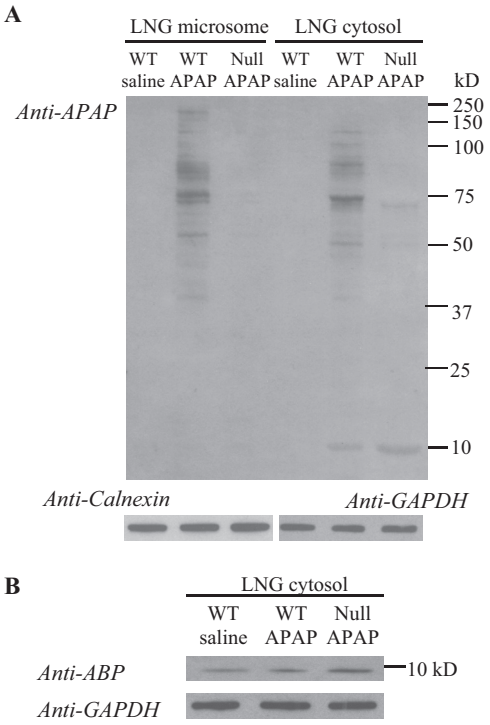

Fig. 7. Immunoblot detection of APAP-protein adducts in the LNG of APAP-treated mice. Two-month-old male mice were fasted overnight before an injection of APAP (at 400 mg/kg i.p.); mice in the control group were treated with saline. Microsomal and cytosol preparations were obtained from the pooled LNGs of four mice; tissues were obtained at 2 h after the APAP treatment. Microsomal and cytosol (A) samples (20 and 30 μg of protein, respectively, in each lane), from either B6 WT or *Cyp2a5*-null (Null) mice, were analyzed on 10% SDS-polyacrylamide gels, and APAP adducts were detected on immunoblots by using a polyclonal anti-APAP antiserum. B, the levels of ABP protein were determined on a separate blot for the same cytosol samples that were used in A to demonstrate induction of the ABP protein in the *Cyp2a5*-null mice. The levels of calnexin (for microsomes, A) and GAPDH (for cytosol, A and B) were also determined, after stripping of the blot to remove the anti-APAP or anti-ABP antibodies, for demonstration of equal protein loading among the three samples. Densitometric analysis (not shown) indicated a ~2.5-fold higher level of APAP-ABP (A) and a 2.8-fold higher level of ABP (B) in the LNG cytosol from APAP-treated *Cyp2a5*-null mice, compared with APAP-treated WT mice.

Discussion

The discovery that *Cyp2a5* deletion leads to significant increases in testosterone levels in the LNG indicates that CYP2A5 is the major enzyme for testosterone metabolism in the LNG. The effects of *Cyp2a5* knockout on testosterone homeostasis in the LNG is tissue-specific, given the lack of a significant change in overall rates of hepatic testosterone metabolism and in circulating testosterone levels (Zhou et al., 2010). Viewed from a mechanistic standpoint, the tissue-specific impact of *Cyp2a5* knockout on testosterone homeostasis in the LNG is clearly related to the dependence of the LNG, but not the liver, on CYP2A5 for testosterone degradation. Considering the fact that CYP2A5 is expressed in numerous other tissues, including kidney, brain, small intestine, olfactory mucosa, lung, other parts of the respiratory tract, and the salivary and lacrimal glands (Piras et al., 2003; Su and Ding, 2004), it will be interesting to determine whether androgen metabolism and homeostasis is altered in other organs of the *Cyp2a5*-null mice. It is noteworthy that of the two human orthologs of mouse CYP2A5, CYP2A13 is also efficient in catalyzing testosterone hydroxylation (von Weymarn et al., 2005), whereas CYP2A6 is not active in this reaction (Liu et al., 1996); the role of human CYP2A13 in androgen metabolism and homeostasis remains to be explored.

The molecular mechanism responsible for the up-regulation of ABP expression in the LNG of male *Cyp2a5*-null mice is not clear at this point; however, the up-regulation seems to be pretranslational, given the increased ABP mRNA levels in the null mice. Testosterone-stimulated synthesis and secretion of steroid hormone (androgen) binding protein (a protein unrelated to ABP) has been reported in Sertoli cells of testes (Louis and Fritz, 1977). Currently, we do not know whether ABP expression in the LNG can be activated by testosterone, despite the observed positive correlation between serum testosterone levels and LNG ABP abundance among adult male mice. Furthermore, it remains to be determined whether the abundance of ABP is also a critical factor for the elevated testosterone level in the LNG of the *Cyp2a5*-null mice. As we had suggested previously, a decrease in testosterone degradation may be necessary, but not sufficient, for an increased accumulation of testosterone in an organ (Zhou et al., 2009). Therefore, additional studies are warranted to further demonstrate activation of ABP expression by testosterone, and to clarify whether the high abundance of testosterone in the LNG of WT mice and the further elevation of testosterone level in the LNG of the *Cyp2a5*-null mice are dependent on ABP.

The up-regulation of ABP subunits provides one direct link between *Cyp2a5* deletion and increased resistance to APAP toxicity in the LNG, given our demonstration that ABP subunits can form conjugates with APAP and thereby protect other cellular proteins and thiol groups against the attack by APAP reactive intermediates. Several salient features of ABP make it an ideal protector against thiol-reactive chemicals: 1) it is abundant in the LNG (~1% total cytosolic protein); 2) it is a secretory protein, thus capable of carrying the conjugated chemical intermediates out of the gland to the nasal mucus; and 3) it contains three cysteine residues per

subunit, so it can quench several reactive molecules at the same time. It is noteworthy that other cysteine-containing secretory proteins may also be able to serve as a protector against thiol-reactive intermediates and, in fact, we observed other proteins that reacted with APAP antibody in microsomes and cytosol, as expected based on previous findings in other tissues (e.g., Gu et al., 2005). Nonetheless, other than APAP-ABP, few other APAP-protein adducts were found to be increased in the LNG of APAP-treated *Cyp2a5*-null mice compared with the LNG of APAP-treated WT mice (Fig. 7). This suggests that other secretory proteins do not make a substantial contribution to the increased protection against APAP toxicity in the LNG of *Cyp2a5*-null mice.

ABP up-regulation alone may not fully explain the nearly total protection of the LNG against APAP-induced tissue damage and nonprotein thiol depletion in the *Cyp2a5*-null mice. Two other factors might also have been important. First, APAP levels in the LNG were significantly decreased in the *Cyp2a5*-null LNG compared with the WT LNG, whereas circulating APAP levels were not different in the two mouse strains; this decrease in LNG APAP bioavailability would reduce the amounts of *N*-acetyl-*p*-benzoquinoneimine produced in situ and thus contribute to a reduction in adduct formation and in toxicity. Second, APAP-GSH levels in the LNG were substantially lower in the *Cyp2a5*-null LNG than in the WT LNG, whereas circulating APAP-GSH levels were not different in the two mouse strains. It is known that APAP-GSH, through its degradation product APAP-Cys, can enter the γ-glutamyl cycle and cause depletion of GSH (e.g., Stern et al., 2005a). Thus, a decrease in APAP-GSH level would reduce the extent of GSH depletion and increase resistance of the tissue to APAP toxicity. In this connection, the ability of liver-generated APAP-GSH and APAP-Cys to induce toxicity in the kidney is well documented (Stern et al., 2005a, 2005b).

The mechanistic link between *Cyp2a5* deletion and the reduction in levels of APAP and APAP-GSH in the LNG remains to be identified. We speculate that the up-regulation of testosterone levels led to an increased rate of excretion of cytosolic content (including APAP and APAP-GSH) from the *Cyp2a5*-null LNG compared with the WT LNG. In this connection, it has been reported by others that testosterone can stimulate secretion from rat lacrimal glands (Sullivan et al., 1990). For APAP, which is lipid-soluble and thus readily absorbed, neither circulating levels nor rates of local metabolism were altered; therefore, the reduced LNG APAP level is most likely due to increased rate of excretion. The decrease in LNG APAP level would contribute to a decrease in LNG APAP-GSH level. However, given the low rates of in situ APAP metabolism, and the likelihood of a transfer of circulating APAP-GSH to the LNG, as implied by our earlier finding that APAP toxicity in the LNG is partly dependent on APAP metabolism in the liver (Gu et al., 2005), it is conceivable that an increase in APAP-GSH excretion from the LNG might have been the more dominant mechanism. On the other hand, the levels of APAP-G and APAP-S were not different in *Cyp2a5*-null and WT mice, a result that argues against an increase in excretion. However, differential transport of the various APAP conjugates has been reported in other organ systems (e.g., Chen et al., 2003). It is possible that, in the LNG, APAP-G and APAP-S are transported more into the blood, whereas APAP and APAP-GSH are more affected by excretion to the nasal mucus. The excretion may have been more affected by CYP2A5-mediated changes in testosterone homeostasis. In any case, further studies on the ability of testosterone to stimulate LNG excretion and to influence tissue burden of APAP and various APAP metabolites are warranted.

Based on our findings, we propose a unique antitoxicant mechanism involving CYP2A5-mediated androgen metabolism in the LNG (Fig. 8). In situ metabolic activation of APAP in the LNG (presumably mediated by CYP2E1) leads to the formation of the reactive *N*-acetyl-*p*-benzoquinoneimine, which forms conjugates with GSH or adducts at cysteine residues on proteins (including ABP) and eventually leads to cytotoxicity. APAP-

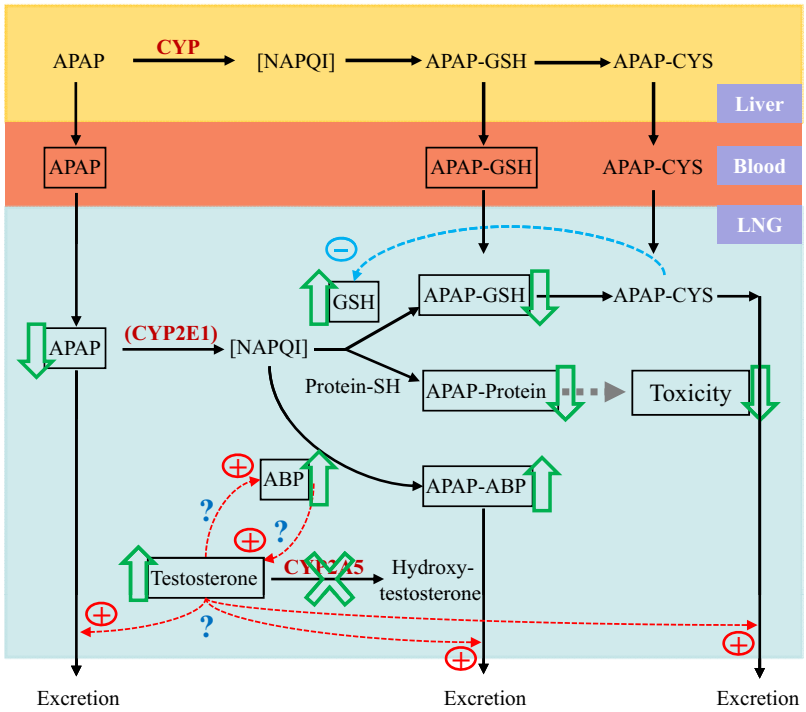

Fig. 8. A proposed novel defensive mechanism against APAP toxicity in the male mouse LNG. Boxed items represent entities measured in APAP-treated mice. Boxed arrows indicate direction of changes observed in *Cyp2a5*-null mice. In situ metabolic activation of APAP in the LNG (presumably mediated by CYP2E1) leads to the formation of the reactive *N*-acetyl-*p*-benzoquinoneimine (NAPQI), which forms conjugates with GSH or protein (including ABP) and eventually leads to cytotoxicity. APAP-GSH and APAP-Cys, either locally formed or absorbed from systemic circulation, cause further depletion of GSH (through the γ-glutamyl cycle) and thus increase vulnerability of cellular proteins to attack by *N*-acetyl-*p*-benzoquinoneimine. In this figure, we speculate that testosterone is a positive regulator of ABP expression and possibly mucus secretion; however, as the "?" indicates, this has yet to be confirmed. LNG testosterone level is regulated negatively by CYP2A5 and positively by ABP. Genetic ablation (or xenobiotic inhibition) of CYP2A5 leads to suppression of testosterone disposition in the LNG, consequent increases in tissue testosterone levels, up-regulation of ABP, and enhanced protection against APAP toxicity through increased formation of APAP-ABP adducts, reduced depletion of cellular GSH, reduced formation of APAP conjugates with other cellular proteins, and (presumably) increased excretion of APAP and APAP-GSH/APAP-Cys to nasal mucus.

GSH and APAP-Cys, either locally formed or absorbed from systemic circulation, cause further depletion of GSH (through the γ-glutamyl cycle) and thus increase vulnerability of cellular proteins to attacks by *N*-acetyl-*p*-benzoquinoneimine. Testosterone, which is abundant in the LNG, may be a positive regulator of ABP expression and possibly mucus secretion; however, LNG testosterone level is regulated negatively by CYP2A5 (through metabolism) and positively by ABP (through direct binding and sequestration). Genetic ablation of *Cyp2a5* leads to suppression of testosterone disposition in the LNG, thus causing increases in tissue testosterone levels, up-regulation of ABP, and enhanced protection against APAP toxicity. Protection occurs through increased formation of APAP-ABP adducts, reduced depletion of cellular GSH, reduced formation of APAP conjugates with other cellular proteins, and reduced tissue burden of APAP and APAP-GSH; the decrease in APAP and APAP-GSH is achieved at least partly through increased excretion of APAP and APAP-GSH/APAP-Cys to nasal mucus. As a further extension of this mechanism, xenobiotic inhibition of CYP2A5 (or other androgen-metabolizing enzymes) may also lead to suppression of testosterone disposition, which may initiate an adaptive response, as seen in the *Cyp2a5*-null mice, for enhanced protection against potential xenobiotic toxicity in the LNG (and possibly other secretory glands or organs). We have no direct evidence for aspects of this model; however, further confirmation and characterization of this putative, novel defensive mechanism, which may be exploited for prevention of xenobiotic toxicity, are under way.

It should be noted that the proposed antitoxicant mechanism is based on studies with male mice. It remains to be determined whether the exact same mechanism also applies to female mice. Female *Cyp2a5*-null mice also showed up-regulation of ABP expression and increased resistance to APAP toxicity in the LNG, compared with WT female mice (X. Zhou and X. Ding, unpublished results). However, it is not clear whether testosterone, which is at much lower abundance in female mice than in males, or progesterone, another ABP ligand, which is abundant in female mice, is involved.

Acknowledgments

We thank Drs. Xiuling Zhang, Cheng Fang, and Jaime D'Agostino of the Wadsworth Center and Dr. Lindsay Hough of the Albany Medical College for helpful discussions, and Weizhu Yang for technical assistance. We gratefully acknowledge the use of the Transgenic and Knockout Mouse Core, the Microarray Core, the Biochemistry Core, and the Histopathology Core of the Wadsworth Center.

Authorship Contributions

Participated in research design: Zhou and Ding.

Conducted experiments: Zhou, Wei, Xie, Kluetzman, Gu, and Zhang.

Contributed new reagents or analytic tools: Laukaitis, Karn, and Roberts.

Performed data analysis: Zhou and Ding.

Wrote or contributed to the writing of the manuscript: Zhou, Laukaitis, Karn, Roberts, and Ding.

References

Chen C, Hennig GE, and Manautou JE (2003) Hepatobiliary excretion of acetaminophen glutathione conjugate and its derivatives in transport-deficient (TR$^-$) hyperbilirubinemic rats. *Drug Metab Dispos* **31:**798–804.

Ding X and Coon MJ (1990) Immunochemical characterization of multiple forms of cytochrome P-450 in rabbit nasal microsomes and evidence for tissue-specific expression of P-450s NMa and NMb. *Mol Pharmacol* **37:**489–496.

Ding X and Coon MJ (1994) Steroid metabolism by rabbit olfactory-specific P450 2G1. *Arch Biochem Biophys* **315:**454–459.

Dlouhy SR, Nichols WC, and Karn RC (1986) Production of an antibody to mouse salivary androgen binding protein (ABP) and its use in identifying a prostate protein produced by a gene distinct from Abp. *Biochem Genet* **24:**743–763.

Dlouhy SR, Taylor BA, and Karn RC (1987) The genes for mouse salivary androgen-binding protein (ABP) subunits alpha and gamma are located on chromosome 7. *Genetics* **115:**535–543.

Getchell ML and Mellert TK (1991) Olfactory mucus secretion, in *Smell and Taste in Health and Disease* (Getchell TV, Doty RL, Bartoshuk LM, and Snow JB Jr eds), pp 83–95, Raven Press, New York.

Gu J, Zhang QY, Genter MB, Lipinskas TW, Negishi M, Nebert DW, and Ding X (1998) Purification and characterization of heterologously expressed mouse CYP2A5 and CYP2G1: role in metabolic activation of acetaminophen and 2,6-dichlorobenzonitrile in mouse olfactory mucosal microsomes. *J Pharmacol Exp Ther* **285:**1287–1295.

Gu J, Dudley C, Su T, Spink DC, Zhang QY, Moss RL, and Ding X (1999) Cytochrome P450 and steroid hydroxylase activity in mouse olfactory and vomeronasal mucosa. *Biochem Biophys Res Commun* **266:**262–267.

Gu J, Cui H, Behr M, Zhang L, Zhang QY, Yang W, Hinson JA, and Ding X (2005) In vivo mechanisms of tissue-selective drug toxicity: effects of liver-specific knockout of the NADPH-cytochrome P450 reductase gene on acetaminophen toxicity in kidney, lung, and nasal mucosa. *Mol Pharmacol* **67:**623–630.

Hinson JA, Reid AB, McCullough SS, and James LP (2004) Acetaminophen-induced hepatotoxicity: role of metabolic activation, reactive oxygen/nitrogen species, and mitochondrial permeability transition. *Drug Metab Rev* **36:**805–822.

Karn RC (1998) Steroid binding by mouse salivary proteins. *Biochem Genet* **36:**105–117.

Karn RC and Laukaitis CM (2003) Characterization of two forms of mouse salivary androgen-binding protein (ABP): implications for evolutionary relationships and ligand-binding function. *Biochemistry* **42:**7162–7170.

Karn RC and Russell R (1993) The amino acid sequence of the alpha subunit of mouse salivary androgen-binding protein (ABP), with a comparison to the partial sequence of the beta subunit and to other ligand-binding proteins. *Biochem Genet* **31:**307–319.

Köntgen F, Süss G, Stewart C, Steinmetz M, and Bluethmann H (1993) Targeted disruption of the MHC class II Aa gene in C57BL/6 mice. *Int Immunol* **5:**957–964.

Lakso M, Pichel JG, Gorman JR, Sauer B, Okamoto Y, Lee E, Alt FW, and Westphal H (1996) Efficient *in vivo* manipulation of mouse genomic sequences at the zygote stage. *Proc Natl Acad Sci USA* **93:**5860–5865.

Laemmli UK (1970) Cleavage of structural proteins during the assembly of the head of bacteriophage T4. *Nature* **227:**680–685.

Laukaitis CM, Heger A, Blakley TD, Munclinger P, Ponting CP, and Karn RC (2008) Rapid bursts of androgen-binding protein (Abp) gene duplication occurred independently in diverse mammals. *BMC Evol Biol* **8:**46–62.

Lee JK, Abe K, Bridges AS, Patel NJ, Raub TJ, Pollack GM, and Brouwer KL (2009) Sex-dependent disposition of acetaminophen sulfate and glucuronide in the in situ perfused mouse liver. *Drug Metab Dispos* **37:**1916–1921.

Liu C, Zhuo X, Gonzalez FJ, and Ding X (1996) Baculovirus-mediated expression and characterization of rat CYP2A3 and human CYP2a6: role in metabolic activation of nasal toxicants. *Mol Pharmacol* **50:**781–788.

Louis BG and Fritz IB (1977) Stimulation by androgens of the production of androgen binding protein by cultured sertoli cells. *Mol Cell Endocrinol* **7:**9–16.

Moe H and Bojsen-Moller F (1971) The fine structure of the lateral nasal gland (Steno's gland) of the Rat. *J Ultrastruct Res* **36:**127–148.

Patten CJ, Thomas PE, Guy RL, Lee M, Gonzalez FJ, Guengerich FP, and Yang CS (1993) Cytochrome P450 enzymes involved in acetaminophen activation by rat and human liver microsomes and their kinetics. *Chem Res Toxicol* **6:**511–518.

Pes D, Mameli M, Andreini I, Krieger J, Weber M, Breer H, and Pelosi P (1998) Cloning and expression of odorant-binding proteins Ia and Ib from mouse nasal tissue. *Gene* **212:**49–55.

Piras E, Franzén A, Fernández EL, Bergström U, Raffalli-Mathieu F, Lang M, and Brittebo EB (2003) Cell-specific expression of CYP2A5 in the mouse respiratory tract: effects of olfactory toxicants. *J Histochem Cytochem* **51:**1545–1555.

Potter DW, Pumford NR, Hinson JA, Benson RW, and Roberts DW (1989) Epitope characterization of acetaminophen bound to protein and nonprotein sulfhydryl groups by an enzyme-linked immunosorbent assay. *J Pharmacol Exp Ther* **248:**182–189.

Roberts DW, Pumford NR, Potter DW, Benson RW, and Hinson JA (1987) A sensitive immunochemical assay for acetaminophen-protein adducts. *J Pharmacol Exp Ther* **241:**527–533.

Stern ST, Bruno MK, Horton RA, Hill DW, Roberts JC, and Cohen SD (2005a) Contribution of acetaminophen-cysteine to acetaminophen nephrotoxicity II. Possible involvement of the gamma-glutamyl cycle. *Toxicol Appl Pharmacol* **202:**160–171.

Stern ST, Bruno MK, Hennig GE, Horton RA, Roberts JC, and Cohen SD (2005b) Contribution of acetaminophen-cysteine to acetaminophen nephrotoxicity in CD-1 mice: I. Enhancement of acetaminophen nephrotoxicity by acetaminophen-cysteine. *Toxicol Appl Pharmacol* **202:**151–159.

Su T and Ding X (2004) Regulation of the cytochrome P450 2A genes. *Toxicol Appl Pharmacol* **199:**285–294.

Sullivan DA, Kelleher RS, Vaerman JP, and Hann LE (1990) Androgen regulation of secretory component synthesis by lacrimal gland acinar cells in vitro. *J Immunol* **145:**4238–4244.

Tonge RP, Kelly EJ, Bruschi SA, Kalhorn T, Eaton DL, Nebert DW, and Nelson SD (1998) Role of CYP1A2 in the hepatotoxicity of acetaminophen: investigations using Cyp1a2 null mice. *Toxicol Appl Pharmacol* **153:**102–108.

von Weymarn LB, Zhang QY, Ding X, and Hollenberg PF (2005) Effects of 8-methoxypsoralen on cytochrome P450 2A13. *Carcinogenesis* **26:**621–629.

Wada R, Tifft CJ, and Proia RL (2000) Microglial activation precedes acute neuro-

degeneration in Sandhoff disease and is suppressed by bone marrow transplantation. *Proc Natl Acad Sci USA* **97:**10954–10959.
Weng Y, DiRusso CC, Reilly AA, Black PN, and Ding X (2005) Hepatic gene expression changes in mouse models with liver-specific deletion or global suppression of the NADPH-cytochrome P450 reductase gene mechanistic implications for the regulation of microsomal cytochrome P450 and the fatty liver phenotype. *J Biol Chem* **280:**31686–31698.
Wijnholds J, Mol CA, van Deemter L, de Haas M, Scheffer GL, Baas F, Beijnen JH, Scheper RJ, Hatse S, De Clercq E, et al. (2000) Multidrug-resistance protein 5 is a multispecific organic anion transporter able to transport nucleotide analogs. *Proc Natl Acad Sci USA* **97:**7476–7481.
Young JT (1981) Histopathologic examination of the rat nasal cavity. *Fundam Appl Toxicol* **1:**309–312.
Zhang X, Zhang QY, Liu D, Su T, Weng Y, Ling G, Chen Y, Gu J, Schilling B, and Ding X (2005) Expression of cytochrome P450 and other biotransformation genes in fetal and adult human nasal mucosa. *Drug Metab Dispos* **33:**1423–1428.
Zhou X, Zhang X, Weng Y, Fang C, Kaminsky L, and Ding X (2009) High abundance of testosterone and salivary androgen-binding protein in the lateral nasal gland of male mice. *J Steroid Biochem Mol Biol* **117:**81–86.
Zhou X, Zhuo X, Xie F, Kluetzman K, Shu YZ, Humphreys WG, and Ding X (2010) Role of CYP2A5 in the clearance of nicotine and cotinine: insights from studies on a *Cyp2a5*-null mouse model. *J Pharmacol Exp Ther* **332:**578–587.
Zhuo X, Gu J, Behr MJ, Swiatek PJ, Cui H, Zhang QY, Xie Y, Collins DN, and Ding X (2004) Targeted disruption of the olfactory mucosa-specific Cyp2g1 gene: impact on acetaminophen toxicity in the lateral nasal gland, and tissue-selective effects on Cyp2a5 expression. *J Pharmacol Exp Ther* **308:**719–728.

Address correspondence to: Dr. Xinxin Ding, Wadsworth Center, New York State Department of Health, Empire State Plaza, Box 509, Albany, NY 12201-0509. E-mail: xding@wadsworth.org